6-22-2009

In situ high energy x-ray synchrotron diffraction study of the synthesis and stoichiometry of LaFeAsO and LaFeAsO1−xFy

R. William McCallum
Iowa State University, mccallum@ameslab.gov

J.-Q. Yan
Iowa State University

Gustav E. Rustan
Iowa State University, grustan@iastate.edu

E. D. Mun
Iowa State University

Yogesh Singh
Iowa State University

In situ high energy x-ray synchrotron diffraction study of the synthesis and stoichiometry of LaFeAsO and LaFeAsO1–xFy

Abstract

The reaction path for the synthesis of LaFeAsO and $LaFeAsO_{1-x}F_y$ by solid state reaction was studied by *in situ* high temperature x-ray diffraction technique and differential thermal analysis in the temperature interval 100 °C $\leqslant T \leqslant$ 1150 °C. Starting with LaAs, Fe_2O_3, Fe, and LaF_3 as precursors, the results show that the synthesis is characterized by three temperature intervals: (1) Below 500 °C the sequential reduction of Fe_2O_3 and Fe_3O_4takes place through the oxidization of LaAs. Below 400 °C, Fe_2O_3 is reduced to Fe_3O_4 by LaAs and then at 400 °C<<em>T<500 >°C Fe_3O_4 is further reduced to Fe. (2) In the temperature interval 500 °C<<em>T<800 >°C, multiple intermediate reactions take place resulting in the formation of FeAs and La_2O_3. (3) The formation of LaFeAsO based phase could be unambiguously resolved above 800 °C. For both LaFeAsO and $LaFeAsO_{1-x}F_y$, FeAs is a primary impurity at high temperatures that melts at ~ 1040 °C. Possible reaction pathways and the difference between F-free and F-doped samples are discussed.

Keywords

Physics and Astronomy, Materials Science and Engineering, differential thermal analysis, fluorine, high-temperature superconductors, impurities, iron compounds, lanthanum compounds, materials preparation, oxidation, reduction (chemical), stoichiometry, X-ray diffraction

Disciplines

Condensed Matter Physics | Metallurgy

Comments

The following article appeared in *Journal of Applied Physics* 105 (2009): 123912, and may be found at http://dx.doi.org/10.1063/1.3149773.

Authors

R. William McCallum, J.-Q. Yan, Gustav E. Rustan, E. D. Mun, Yogesh Singh, S. Das, R. Nath, Sergey L. Bud'ko, Kevin W. Dennis, David C. Johnston, Paul C. Canfield, Matthew J. Kramer, Andreas Kreyssig, Thomas A. Lograsso, and Alan I. Goldman

AIP | Journal of Applied Physics

In situ high energy x-ray synchrotron diffraction study of the synthesis and stoichiometry of LaFeAsO and LaFeAsO1−xFy

R. W. McCallum, J.-Q. Yan, G. E. Rustan, E. D. Mun, Yogesh Singh et al.

Citation: J. Appl. Phys. **105**, 123912 (2009); doi: 10.1063/1.3149773
View online: http://dx.doi.org/10.1063/1.3149773
View Table of Contents: http://jap.aip.org/resource/1/JAPIAU/v105/i12
Published by the AIP Publishing LLC.

In situ high energy x-ray synchrotron diffraction study of the synthesis and stoichiometry of LaFeAsO and $LaFeAsO_{1-x}F_y$

R. W. McCallum,[1,2,a)] J.-Q. Yan,[1] G. E. Rustan,[1,3] E. D. Mun,[1,3] Yogesh Singh,[1,3] S. Das,[1,3] R. Nath,[1] S. L. Bud'ko,[1] K. W. Dennis,[1] D. C. Johnston,[1,3] P. C. Canfield,[1,3] M. J. Kramer,[1,2] A. Kreyssig,[1,3] T. A. Lograsso,[1] and A. I. Goldman[1,3]
[1]*Materials Sciences and Engineering, Ames Laboratory, U.S. DOE, Iowa State University, Ames, Iowa 50011, USA*
[2]*Materials Science and Engineering, Iowa State University, Ames, Iowa 50011, USA*
[3]*Department of Physics and Astronomy, Iowa State University, Ames, Iowa 50011, USA*

(Received 11 March 2009; accepted 10 May 2009; published online 22 June 2009)

The reaction path for the synthesis of LaFeAsO and $LaFeAsO_{1-x}F_y$ by solid state reaction was studied by *in situ* high temperature x-ray diffraction technique and differential thermal analysis in the temperature interval $100\ ^\circ C \leqslant T \leqslant 1150\ ^\circ C$. Starting with LaAs, Fe_2O_3, Fe, and LaF_3 as precursors, the results show that the synthesis is characterized by three temperature intervals: (1) Below 500 °C the sequential reduction of Fe_2O_3 and Fe_3O_4 takes place through the oxidization of LaAs. Below 400 °C, Fe_2O_3 is reduced to Fe_3O_4 by LaAs and then at $400\ ^\circ C < T < 500\ ^\circ C$ Fe_3O_4 is further reduced to Fe. (2) In the temperature interval $500\ ^\circ C < T < 800\ ^\circ C$, multiple intermediate reactions take place resulting in the formation of FeAs and La_2O_3. (3) The formation of LaFeAsO based phase could be unambiguously resolved above 800 °C. For both LaFeAsO and $LaFeAsO_{1-x}F_y$, FeAs is a primary impurity at high temperatures that melts at ~1040 °C. Possible reaction pathways and the difference between F-free and F-doped samples are discussed.
 [DOI: 10.1063/1.3149773]

I. INTRODUCTION

The discovery of high transition temperature (T_c) superconductivity with structural units of (FeAs) layers has attracted extensive attention in the scientific community.[1] Like the cuprates, this series of materials share a common structural feature, in this case the (FeAs) layers. However, in these materials, the planes may be separated by either oxide layers, such as $RO_{1-x}F_x$ in $RFeAsO_{1-x}F_x$ (R=light rare earth element), or metallic layers, such as AE metal in $AE_{1-x}K_xFe_2As_2$ (AE=Ca, Sr, or Ba) and Li in LiFeAs, offering the opportunity to study superconductivity in both oxides and intermetallics in closely related compounds. This may serve as a bridge in the understanding of the superconductivity in high temperature oxide superconductors as compared to conventional intermetallic superconductors. Although they were discovered later, the pseudoternary K-doped $AEFe_2As_2$ compounds are easier to prepare and, in fact, millimeter sized single crystals have been grown by flux method or Bridgman technique.[2–6] In contrast, the preparation of polycrystalline $RFeAsO_{1-x}F_x$ has been plagued by high levels of irreproducibility characterized by large run to run variations in phase purity and superconducting fraction.

Conventional solid state reaction has been widely used to synthesize $RFeAsO_{1-x}F_x$ compounds. The most common synthesis routes utilize one of two different sets of starting materials.

(1) Introducing oxygen by R_2O_3,[1]

$$1/3R_2O_3 + 1/3R + FeAs \rightarrow ROFeAs, \tag{1a}$$

$$(1-x)/3R_2O_3 + x/3RF_3 + (1+x)/3R + FeAs \rightarrow RFeAsO_{1-x}F_x. \tag{1b}$$

(2) Introducing oxygen by Fe_2O_3,[7]

$$RAs + 1/3Fe_2O_3 + 1/3Fe \rightarrow RFeAsO, \tag{1c}$$

$$(1-x/3)RAs + x/3RF_3 + (1-x)/3Fe_2O_3 + (1+2x)/3Fe + x/3As \rightarrow RFeAsO_{1-x}F_x. \tag{1d}$$

While we have observed no significant difference in phase purity between the above two sets, it is generally believed that the high stability of rare earth oxides may hinder the reaction. Thus most syntheses were performed starting with RAs. Besides the majority RFeAsO phase, R_2O_3 and FeAs have generally been observed as impurities when synthesizing RFeAsO regardless of the starting materials.[1,7,8] $La_{4.67}(SiO_4)_3O$ and Fe_2As have also been reported as impurities in some syntheses.[9] In F-doped compositions, ROF has been observed as impurity. The existence of ROF signals that the F-doping in the majority phase should be different from the nominal one resulting in a composition of $RFeAsO_{1-x}F_y$ for F-doped samples where $y < x$. Despite the tremendous amount of work on the physical properties of $RFeAsO_{1-x}F_x$, a detailed understanding of the formation of these impurities and the reaction path to the desired phase remains elusive.

The formation of single-phase RFeAsO and $RFeAsO_{1-x}F_y$ presents a number of technical problems. The root cause of these problems is the fact that three to five reactants must be combined into a homogenous sample. In addition, the low melting temperature of Fe–As binary compounds was viewed as a possible source of phase segregation

a)Electronic mail: mccallum@ameslab.gov.

during preparation when liquid is formed and migrates under the influence of capillary forces, temperature gradients, and gravity.[10] Given the fact that R_2O_3, RF_3, *R*OF, *R*As, and Fe_2O_3 all melt above 1500 °C, the diffusion of the refractory components is expected to be limited below the melting of the Fe–As phase mixtures between 840 and 1040 °C.

In order to gain a more complete understanding of the sample preparation of $RFeAsO_{1-x}F_y$ materials, we have undertaken a detailed study of the reaction route in both undoped and fluorine doped LaFeAsO. This study utilized both differential thermal analysis (DTA) and *in situ* high temperature x-ray diffraction. High energy x-rays from a synchrotron allow for data to be taken in transmission geometry so that the bulk of the sample is measured. The use of a charge coupled device (CCD) area detector allows the acquisition of high quality diffraction patterns in time slices as short as 20 s. This rapid acquisition rate, coupled with continuous heating, allows for a real time determination of phases and phase distributions as a function of temperature that can be correlated with thermal analysis measurements. In this way, the reaction pathway for a given set of starting materials is determined including the formation and elimination of intermediate phases leading in turn to the formation of the $RFeAsO_{1-x}F_y$ phase. Residual impurity phases are also identified.

From the analysis of the high temperature diffraction data, we have determined the phase evolution as a function of temperature in the formation of the FeAs-based superconductors $LaFeAsO_{1-x}$ and $LaFeAsO_{1-x}F_y$ under ambient pressure conditions. Based on the analysis of the phase evolution for $LaFeAsO_{1-x}$, we have proposed a reaction path which has significant implications with respect to the formation of single-phase materials. Consistent with thermal analysis results, the control of the reaction in the proximity of the Fe–Fe_2As eutectic at 840 °C is important for controlling the reaction rates and sample homogeneity. From an analysis of the observed phase composition at high temperature, we conclude that the materials may form with a large oxygen deficiency at the reaction temperature. The determination of this oxygen deficiency is highly dependent on the second phases which are present in the fully reacted material. This oxygen deficiency plays a significant role in the phase formation and may control the amount of F which is actually doped into the sample. While this oxygen deficiency controls the ability to make single-phase samples, it also raises significant questions as to the doping of the (FeAs) layers in nominal $RFeAsO_{1-x}F_x$.

II. EXPERIMENTAL DETAILS

Two compositions were studied: Composition A is F-free with LaAs, Fe_2O_3, and Fe as starting materials to form the nominal composition LaFeAsO; composition B has 10% F-doping with LaAs, LaF_3, Fe_2O_3, Fe, and $LaAs_2$ as starting materials proportional to the desired stoichiometry of the $LaFeAsO_{0.9}F_{0.1}$. The As (Alfa Aesar, 99.999%), Fe (JMC, 99.999%), and Fe_2O_3 (Alfa Aesar, 99.998%) were purchased commercially while La and LaF_3 were from the Materials Preparation Center, Ames Laboratory.[11] LaF_3 was prepared from high purity La_2O_3 using anhydrous HF gas. LaAs and $LaAs_2$ were synthesized by reacting pure La filings and As pieces in a quartz ampoule partially filled with Ar. La filings were prepared by filing La metal under N_2 or Ar in a glovebox to prepare particles of roughly 0.1 mm diameter. The small size of the rare earth filings was mandated by the extreme stability of the LaAs compounds, which form a shell around the particle limiting the reaction depth. A slight excess of As, 1%, was used. The ampoule was ramped to 600 °C at the rate of 50 °C/h, held at this temperature for 15 h, and then heated to 910 °C in 3 h and held 10 h. Finally, the ampoule was furnace cooled. Room temperature Cu $K\alpha$ x-ray powder diffraction confirmed that the LaAs and $LaAs_2$ prepared in this manner are single phase.

For both DTA and high temperature x-ray diffraction measurements reported here, standard laboratory preparation conditions were reproduced as closely as possible. The starting materials were weighed in the appropriate ratio and ground together by hand in a mortar and pestle. After thorough mixing, the precursor mixtures were pressed into 0.5 mm diameter by 1.5 mm long pellets using steel dies and tungsten carbide pistons. Due to the small diameter of the pellets required to limit the x-ray absorption, pellets were pressed in a hand arbor press and no accurate value of the pressure was determined. However, based on the mechanical advantage of the arbor press, the pressing force is estimated to be 5–10 kN. The pellets were sealed in 3 mm OD 2 mm ID quartz capillaries between 2 mm quartz rods so that they were held in a restricted geometry to insure that the sample remained in the x-ray beam during heating. All handling of samples including weighing, grinding, and pellet pressing were performed under dry N_2 in a glovebox to insure that there was no exposure to air prior to sealing the capillaries. Special precautions were taken to prevent the exposure of pellets to air while transferring the samples from the glovebox to the gas manifold of the glass bench.

DTA was performed using a Perkin Elmer DTA 7 over the temperature range of 100–1300 °C. The precursor mixtures were sealed in Ta crucibles,[12] using a laser welder which allowed them to be sealed in vacuum. These measurements were performed at a scan rate of 10 °C/min.

The high-energy x-ray diffraction (HEXRD) studies were performed at station 6ID-D in the MUCAT sector at the Advanced Photon Source (APS), Argonne National Laboratory. Silicon double-crystal monochromators were used to select an energy of 99.55 keV, which corresponds to a wavelength of 0.124(1) Å. The use of high-energy x-rays allows the diffraction patterns to be taken in a transmission geometry and the ability to enclose the sample in a controlled atmosphere. The furnace employed is a scaled down version of a typical tube style furnace designed to fit in the Eulerian cradle of the Huber 4-circle goniometer.[13] The furnace is equipped with an ~0.3 mm thick silica liner which was evacuated to a moderate vacuum level using a fore pump then closed off during heating to further protect the environment from possible contamination from As vapor in the event of a sample tube failure. The time resolved HEXRD was obtained using a MAR CCD (MAR Research, Evanston, IL) placed ~808 mm from the sample. The sample to detec-

tor distance was calibrated using a NIST Si (640C) standard. The Debye cones intersect the CCD, and the recorded data are then azimuthally integrated to obtain a one-dimensional (1D) pattern with the software package FIT2D.[14] This geometry was chosen to obtain high reciprocal-space diffraction patterns every 20 s while maintaining a high signal-to-noise ratio to resolve subtle details of the phase transitions at a modest heating rate of 10 °C/min and during isothermal holds. Data were taken as the temperature of the sample was scanned at a rate of 10 °C/min from 20 to 1150 °C, allowing a direct comparison with the DTA measurement with each HEXRD scan having a temperature resolution of ~3 °C. Phases were identified with the software JADE, and Rietveld refinements for particular patterns were carried out with GSAS.[15] Besides the precursor mixture, pellets of all starting binary compositions were also sealed in quartz capillaries and studied with HEXRD for possible phase transitions in the same temperature interval.

III. EXPERIMENTAL RESULTS

A. DTA measurements

DTA measurements performed in capsules sealed under vacuum for both compositions A and B are presented in Fig. 1(a). The vertical dotted lines represent the sublimation temperature of As, slightly reduced from its value of 610 °C for 1 atm pressure, and various melting temperatures from the Fe–As phase diagram.[16] Considering the refractory nature of the starting materials, it was expected that reactions would take place at relatively high temperatures. However, several large exotherms are observed at temperatures below 600 °C. Despite the fact that there is no free As observed in the x-ray diffraction patterns of the precursors, an endotherm is clearly visible at 600 °C, corresponding to the sublimation temperature of As in the F-doped precursors [Fig. 1(b)]. For the F-free precursor, there is a corresponding change of slope on the side of the lower temperature exotherm. For both compositions A and B, there appears to be a small broad exotherm between 600 and 700 °C indicating further reactions. Both doped and undoped compositions exhibit a moderate endotherm at the Fe–Fe_2As eutectic temperature, 840 °C. For the F-doped sample a coupled exotherm-endotherm appears around the melting temperature of Fe_2As at 940 °C, Fig. 1(c). The endotherm is assumed to be associated with the melting of Fe_2As which formed at the As sublimation temperature of ~600 °C, while the formation of more liquid triggers a strong exothermic reaction. In the undoped sample, where there is no endotherm at 940 °C, the exothermic reaction is about 50 °C higher in temperature and is broader. Fe_3As_2 is a high temperature solid solution in the Fe–As phase diagram[16] which is only stable above 824 °C and melts at 1000 °C, where both curves in Fig. 1 exhibit a compound feature containing both an exotherm and an endotherm. No further features were observed above 1050 °C.

The presence of Fe–As compounds in the undoped precursor suggests that the low temperature exotherms at $T < 600$ °C are associated with the oxidation of the LaAs to form La_2O_3 accompanied by the reduction of the Fe_2O_3 and formation of Fe–As compounds. The melting of various Fe–As binary compounds would enhance reaction kinetics and enable rapid phase formation. However, the liquid makes possible the macroscopic phase segregation.[10]

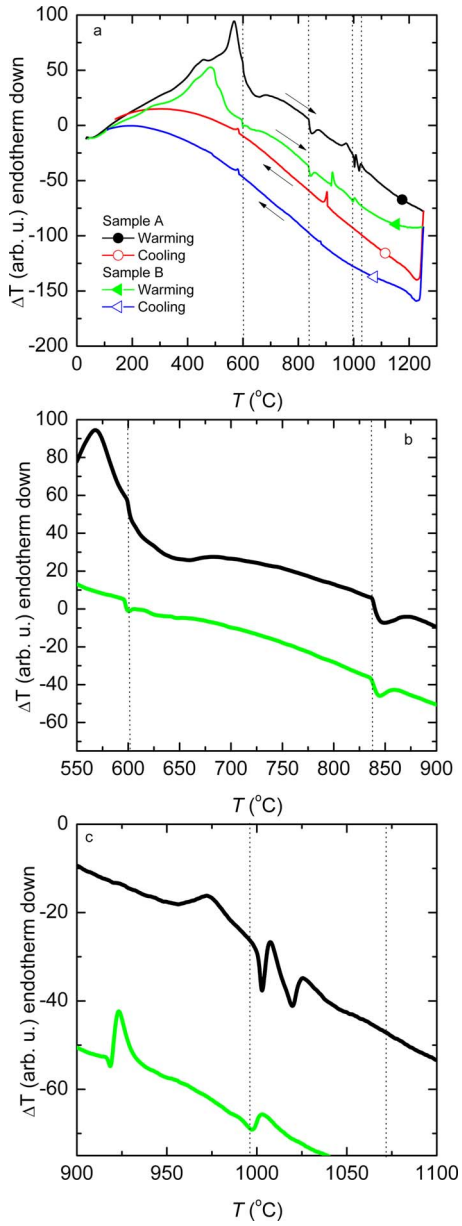

FIG. 1. (Color online) (a) DTA curve, heating and cooling, of composition A: LaAs+1/3Fe_2O_3+1/3 Fe and composition B: LaAs+Fe_2O_3+Fe+LaF_3+$LaAs_2$. [(b) and (c)] Heating curves only for compositions A (upper curve) and B (lower curve).

B. X-ray diffraction

Figure 2(a) shows a typical x-ray diffraction image recorded by CCD detector for composition A at 200 °C. Figure 2(b) shows the corresponding azimuthal angle-integrated diffraction pattern from the recorded image. The angular resolution of the two-dimensional image is limited by the 2048 × 2048 resolution of the CCD. However, the integration over the observed portion of the Debye–Scherrer ring results in an excellent signal-to-noise ratio which allows the detection of very weak peaks in the regions of the pattern where the peaks are well separated. Figure 2(c) shows the azimuthal

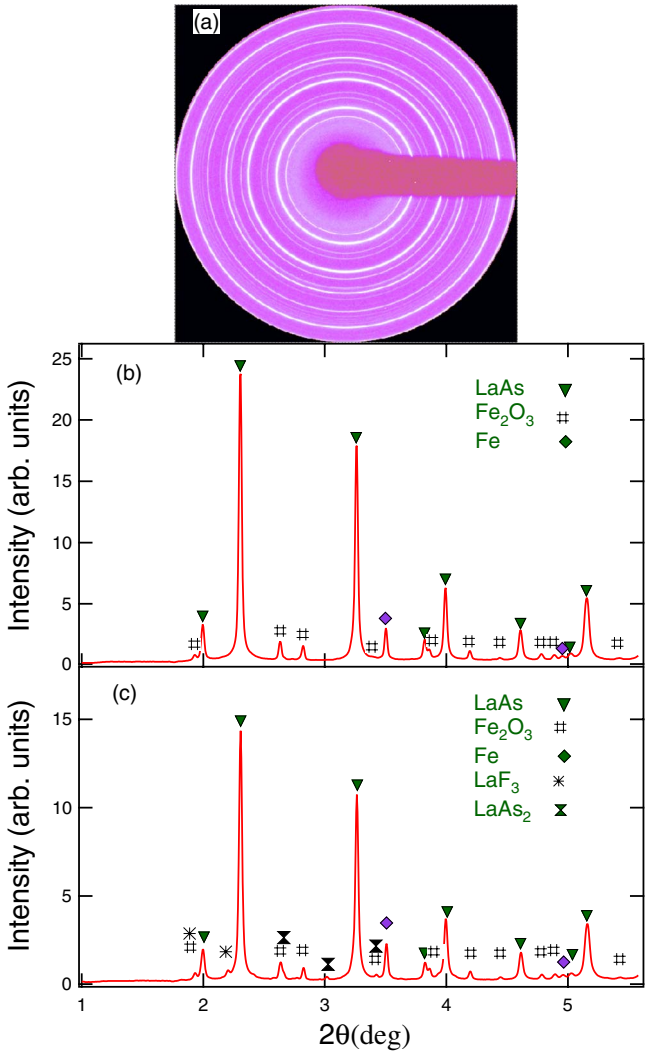

FIG. 2. (Color online) (a) Typical x-ray diffraction image recorded on the CCD detector for composition A at 200 °C. (b) 1D plot of angle-integrated intensity vs 2θ for composition A at 200 °C. (c) 1D plot of angle-integrated intensity vs 2θ for composition B at 100 °C.

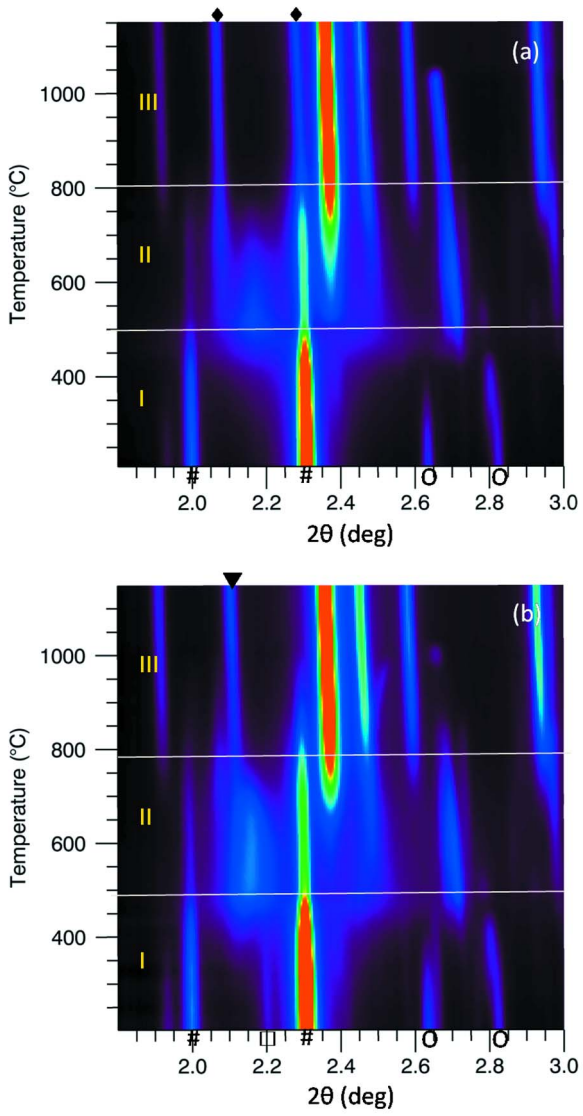

FIG. 3. (Color online) Surface plot of the x-ray diffraction patterns as a function of temperature for (a) composition A and (b) composition B. Three different temperature ranges discussed in text are labeled as I, II, and III, respectively. At the lowest temperature, phases observed in the two theta range are labeled as □ for LaF_3, ○ for Fe_2O_3, and # for LaAs. At 1150 °C, hexagonal La_2O_3 (♦) in (a) and LaOF (▼) in (b) are observed besides LaFeAsO.

angle-integrated diffraction pattern for composition B taken at 100 °C. As shown in Figs. 2(b) and 2(c), all starting materials could be well resolved, confirming that the resolution of the experiment is sufficient to resolve the constituents which is critical for a reliable study of the reaction mechanism.

Figure 3 presents a contour plot of the x-ray diffraction patterns for (a) composition A and (b) composition B. Even without indexing each peak, a casual examination of these data reveals that there are three temperature regimes where reactions are occurring with the clear formation of at least one intermediate phase that appears between 400 and 800 °C for both compositions. The coexistence of multiple, highly disordered phases in the intermediate temperature range makes it extremely difficult to perform quantitative analysis with Rietveld refinements. Thus the diffraction pattern at each temperature was first analyzed with JADE for phase identification and the peak intensity of one typical reflection from each phase was monitored and plotted in Fig. 4 to show quantitatively the evolution with temperature of various phases. The typical reflections were selected to avoid overlap with peaks from other phases. Those reflections are (102) for LaFeAsO, (110) for Fe, (220) for LaAs, (111) for FeAs, (311) for Fe_3O_4, (−315) for $LaAs_2$, (111) for LaF_3, (101) for LaOF, (100) in panel (a) and (102) in panel (b) for hexagonal La_2O_3, and (104) in panel (a) and (116) in panel (b) for Fe_2O_3. Due to the extremely small grain size or a highly disordered structure resulting in diffuse diffraction peaks for the cubic La_2O_3, a shaded area in Fig. 4 was used to describe its formation, growth, and disappearance. For LaF_3, above 475 °C, the (111) diffraction peak overlaps with the strong diffuse peak from cubic La_2O_3, thus the evolution of LaF_3 with temperature above 475 °C could not be determined from our measurements. The temperature dependence of the intensity of each characteristic line for each phase quantitatively describes the temperature dependence of the phase fraction. However, the intensity difference of different

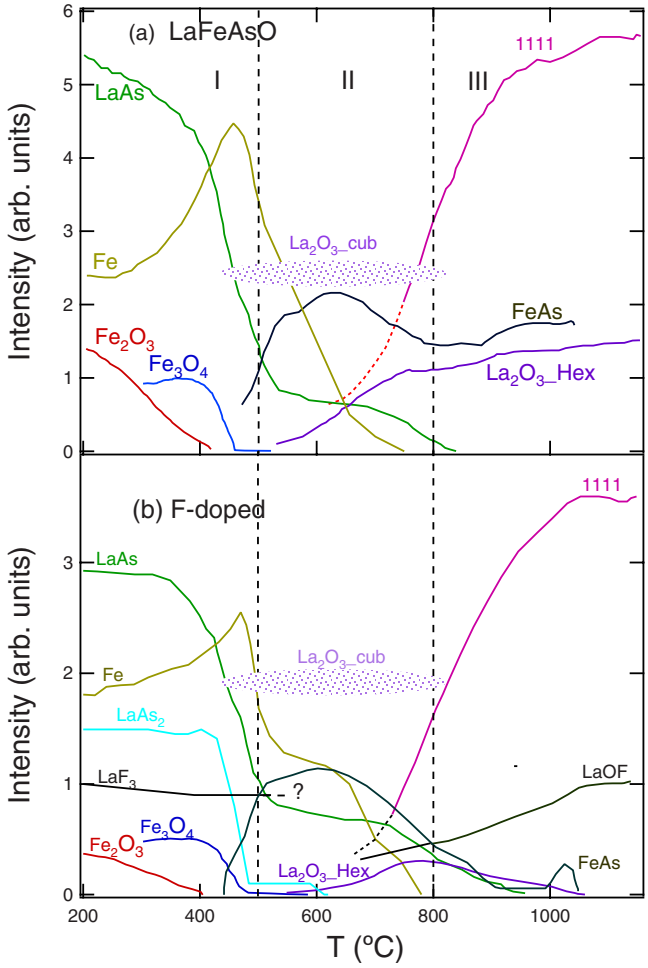

FIG. 4. (Color online) Temperature dependence of diffraction peak intensity of all observed phases for (a) composition A: LaFeAsO and (b) the F-doped composition B. Three temperature intervals as described in the text are denoted with vertical dashed lines.

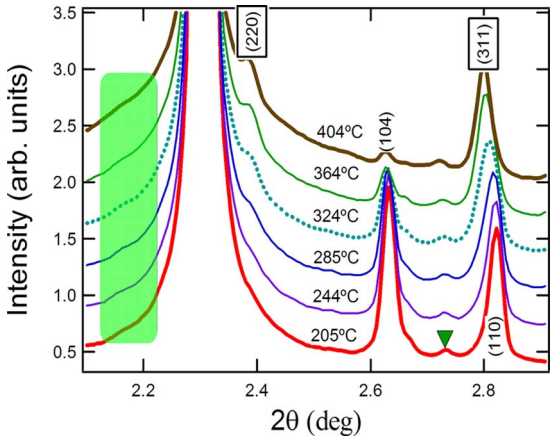

FIG. 5. (Color online) Selected diffraction patterns of sample A in the temperature interval 205 °C$<T<$404 °C highlighting the change of Fe_2O_3 to Fe_3O_4 and the development of diffuse scattering of cubic La_2O_3. Reflections with boxed indices belong to Fe_3O_4, while peaks with indices in parentheses belong only to starting Fe_2O_3. The dashed area highlights the increase in the background close to 2.2° where the (222) peak of cubic La_2O_3 emerges at higher temperatures. The diffraction patterns were shifted vertically for clarity. The weak reflection labeled with a solid triangle is from SiO_2 from the capillary. Reflections from sample B show the same temperature dependence.

phases does not necessarily indicate the differences in relative fraction. Rietveld refinements of the patterns at low and high temperatures were performed to quantitatively estimate the phase fractions.

In the following, we will present the detailed analysis of the diffraction patterns in three different temperature ranges: (I) low temperature range: 100–500 °C; (II) intermediate transition temperature range: 500–800 °C; (III) high temperature range: 800–1150 °C.

1. Low temperature range of 100–500 °C

In this temperature range, both compositions A and B behave similarly. Below 200 °C, all observed peaks could be indexed using the known structures of the starting materials. Above 200 °C, three prominent features are noteworthy.

(1) The starting Fe_2O_3 material is reduced to Fe_3O_4 in the temperature interval 200 °C$<T<$400 °C. Figure 5 presents some typical diffraction patterns in the temperature interval 200 °C$<T<$400 °C from composition A. With increasing temperature, the intensity of the Fe_2O_3 (104) reflection decreases quickly; the Fe_2O_3 (110) peak broadens and is replaced by the (311) peak of Fe_3O_4 above 320 °C. In combination with other diffraction peaks [e.g., (220) at $2\theta\sim2.39°$], this identifies the phase above 320 °C as Fe_3O_4.

(2) Concurrent with the formation of Fe_3O_4, the background around the LaAs (220) peak at $2\theta\sim2.30°$ increases when heating. As further discussed below, the pattern for poorly crystallized cubic La_2O_3 will grow out of this gradually growing background highlighted by the shaded area in Fig. 5. This suggests that while Fe_2O_3 is reduced to Fe_3O_4, LaAs is being oxidized and finally leads to the formation of La_2O_3. We note that $LaAsO_4$ is a known ternary phase and is a possible intermediate phase in the oxidation of LaAs. However, no evidence for this phase is seen in the diffraction patterns. Thus if this intermediate forms, it is poorly crystallized.

(3) In the temperature interval 400 °C$<T<$500 °C in Fig. 4, the intensities of the LaAs (220) and Fe_3O_4 (311) peaks drop quickly with increasing temperature suggesting a reaction between LaAs and Fe_3O_4. Fe_3O_4 disappears around 460 °C in composition A and ~480 °C for composition B. The sharp intensity increase in the Fe (110) peak below 450 °C indicates that the Fe oxides are reduced concurrent with the disappearance of LaAs but prior to the formation of FeAs. Above 450 °C, the intensity of the elemental Fe (110) reflection decreases as FeAs appears. Similarly, in the F-doped composition B, the intensity of the $LaAs_2$ (−315) peak also drops sharply in this temperature interval, while the intensity of the LaF_3 (111) peak remains constant. These data suggest that above 400 °C, the La–As compounds are replaced by the more stable La_2O_3 as the iron oxides are reduced.

(4) At $T\sim450$ °C, FeAs starts to appear in both compositions. Also diffuse scattering from poorly crystallized

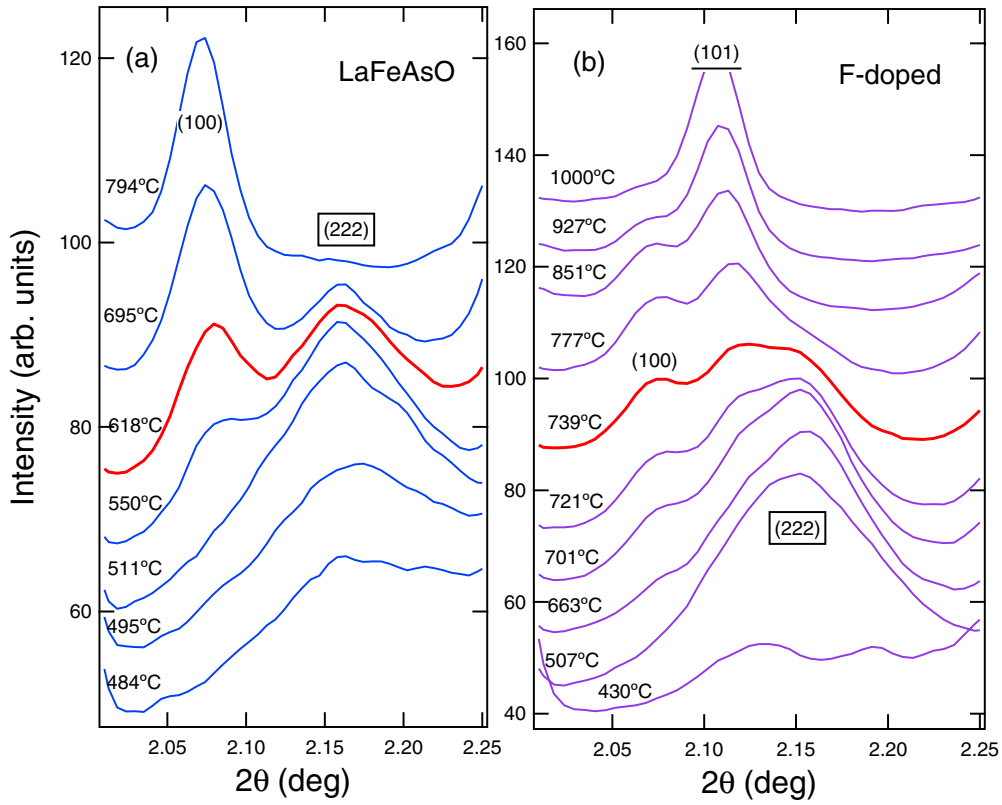

FIG. 6. (Color online) Selected diffraction patterns highlighting the formation of cubic La_2O_3 and hexagonal La_2O_3 in (a) composition A: LaFeAsO and LaOF in (b) composition B: F-doped LaFeAsO. The patterns are shifted vertically for clarity. Characteristic peaks shown are (100) of hexagonal La_2O_3, (222) of cubic La_2O_3, and (101) of LaOF. The red curves highlight the coexistence of cubic La_2O_3, hexagonal La_2O_3, and in F-doped composition B, LaOF.

cubic La_2O_3 can be resolved at ~450 °C in composition A and ~420 °C in composition B.

2. Intermediate temperature range of 500–800 °C

As stated above, the (111) reflection from FeAs becomes observable at $T \sim 450$ °C as shown in Figs. 3 and 4. It is well resolved at ~500 °C. At ~620 °C, the intensity of this reflection reaches a maximum and then starts to decrease with further increasing temperature. The intensity of the LaAs (220) peak shows negligible change in the interval 520 °C $< T <$ 700 °C and then decreases rapidly with increasing temperature above 700 °C. The Fe (110) peak disappears at ~750 °C in composition A and at 780 °C in composition B.

Figure 6(a) shows the evolution of the La_2O_3 diffraction peaks in undoped composition A. The broad (222) peak from cubic La_2O_3 at $2\theta \approx 2.15°$ becomes observable at ~450 °C, and it sharpens with increasing temperature. Around 530 °C, the (100) peak of hexagonal La_2O_3 at $2\theta \approx 2.06°$ appears as a shoulder; it sharpens and the intensity increases while heating. The coexistence of cubic and hexagonal La_2O_3 is well illustrated in Fig. 6(a) by the patterns taken at 550–700 °C. The evolution with temperature and coexistence of cubic La_2O_3, hexagonal La_2O_3, and LaOF are demonstrated in Fig. 6(b) with selected diffraction patterns at specific temperatures. In F-doped composition B, LaF_3 could not be resolved because of peak overlapping above 475 °C. However, the evolution with temperature of the inverse relationship between the peak heights of La_2O_3 and LaOF clearly suggests that LaF_3 reacts with La_2O_3 to form LaOF above 650 °C in composition B. This feature distinguishes composition B from composition A in this temperature range and is consistent with the normal preparation procedure for LaOF which consists of reacting La_2O_3 and LaOF in this temperature range.[17] In F-doped composition B, hexagonal La_2O_3 appears, together with LaOF, at ~660 °C. In both compositions A and B, cubic La_2O_3 disappears around 800 °C.

3. High temperature range of 800–1150 °C

This temperature range is characterized by the rapid development of the LaFeAsO (1111) phase. From Fig. 4, reflections from LaFeAsO become resolvable at ~750 °C in both compositions A and B. The intensity of the (102) peak increases with increasing temperature and saturates above ~1050 °C. At 1040 °C, all reflections from FeAs disappear because FeAs melts. Upon cooling, the FeAs diffractions reappear confirming that the 1040 °C event is the melting of FeAs. This temperature agrees well with the phase diagram.[17] Reflections from LaAs could not be observed above ~900 °C in composition A and ~950 °C in composition B.

The evolution with temperature of hexagonal La_2O_3 and final phases distinguish composition A from B in this temperature interval. In composition A, hexagonal La_2O_3 is stable up to the highest temperature studied (1150 °C), while in composition B, the amount of hexagonal La_2O_3 reaches a maximum at ~820 °C and then gradually decreases with further increase in temperature. Hexagonal La_2O_3 finally dis-

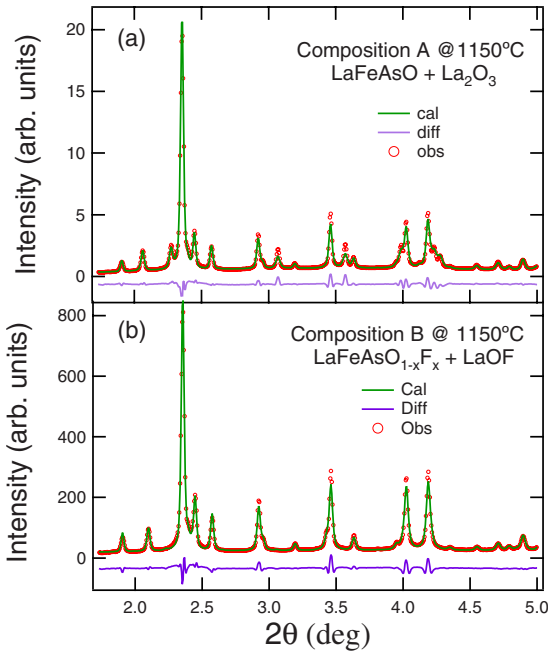

FIG. 7. (Color online) GSAS fitting of the diffraction patterns of compositions A (a) and B (b) taken at 1150 °C. Liquid FeAs impurity is also present but its x-ray diffraction is too diffuse to be observable.

appears at ~1000 °C as shown in Figs. 6(b) and 4(b). The intensity of the LaOF (101) peak follows the temperature dependence of the formation of the 1111 phase: it increases while heating and saturates above 1050 °C. After cooling down to room temperature, the final phases observed are 1111, LaOF, and FeAs. In composition A, the final phases observable in our experiment are 1111, hexagonal La_2O_3, and FeAs. The quality of the data allowed Rietvelt refinement for patterns taken at $T > 1000$ °C.

Figure 7 shows a typical GSAS fit of the diffraction patterns for both compositions. These particular patterns were taken at 1150 °C which is above the melting temperature of FeAs so that it is not visible in the diffraction pattern. When fitting composition A, if the La:Fe:As ratio was allowed to vary from 1:1:1, the fit always returned 1:1:1 within the resolution limit of the fitting so the ratio was fixed to 1:1:1. Varying oxygen occupancy does not significantly improve the fitting, so for the determination of phase fractions the La:Fe:As:O ratio was set to 1:1:1:1. The fit in Fig. 7 is typical of that obtained and has a final average *R*-factor of ~7.0% with an average $\chi^2 \sim 0.25$. Once the relative fraction of each phase was determined by the GSAS fit, the oxygen stoichiometry was estimated from the phase fractions. Similarly for composition B the La:Fe:As ratio was fixed at 1:1:1 in the fitting. If the O and F values were allowed to vary freely, a total occupation of much greater than 1 was obtained for that site. As in the case of composition A, the nominal composition was used in the fitting and a realistic estimate for these values could be obtained by fitting the phase fractions.

IV. DISCUSSION

For the formation of single-phase LaFeAsO and $LaFeAsO_{1-x}F_y$, three to five reactants must be combined into a homogenous sample. Given this number of reactants, it is not possible to have the stoichiometric ratio of elements present at a single contact point allowing for direct formation of the desired compound. Of the common starting materials, La_2O_3, LaF_3, LaOF, LaAs, and Fe_2O_3 all melt above 1500 °C so that the diffusion of the refractory components is expected to be limited. On the other hand, Fe–As phase mixtures display liquid formation between 840 °C, where there is a eutectic between Fe and Fe_2As, and 1040 °C where the highest melting compound FeAs melts congruently. While liquid phases provide rapid diffusion of reaction constituents, they may also result in significant phase segregation due to wetting and surface tension characteristics.[10] Thus it is necessary to control the reaction path in order to provide sufficient surface melting for adequate diffusion without creating macroscopic phase segregation. This requires a detailed knowledge of the reaction path.

A. Reaction path

HEXRD measurements of the individual compounds LaAs and Fe_2O_3 in sealed quartz ampoules confirm that both binary compounds are stable up to 1150 °C. While the partial pressure of As in equilibrium with LaAs is expected to be very low due to the high stability of LaAs, the partial pressure of O_2 in equilibrium with Fe_2O_3 is approximately 10^{-4} atm at 1100 °C.[15] For Fe_2O_3 sealed in vacuum in a low volume ampoule, the amount of Fe_2O_3 which converts to Fe_3O_4 to provide this partial pressure is minimal. However, when LaAs and Fe_2O_3 are sealed in the same ampoule, this allows the possibility of the reaction of O with LaAs. The LaAs serves as an oxygen sink so that a significant amount of Fe_2O_3 can be reduced. This is consistent with the change of Fe_2O_3 to Fe_3O_4 and the enhancement of background around the LaAs (220) reflection. However, the equilibrium partial pressure of O_2 with Fe_2O_3 at 400 °C is significantly below 10^{-14} atm,[18] while the oxygen partial pressures to reduce Fe_3O_4 and FeO at that temperature are even lower. Since the observation of diffuse scattering of cubic La_2O_3 clearly indicates that LaAs is replaced by La_2O_3 while Fe_2O_3 is reduced, we must therefore assume either a solid state reaction between these reactants or that As is functioning as a transport agent. Below 400 °C, Fe_2O_3 can be reduced to Fe_3O_4 by one of three possible routes. An analysis of the total weight percent change in the sample composition for each of these reactions reveals that we can only expect to detect the disappearance of the Fe_2O_3, the appearance of Fe_3O_4, and the reduction in LaAs. The observed reduction in the phase fraction of LaAs is significantly greater than the calculated values for the reactions,

$$Fe_2O_3 + LaAs \rightarrow 2/3Fe_3O_4 + 1/9La_2O_3 + 7/9LaAs + 2/9As, \quad (2a)$$

$$Fe_2O_3 + LaAs \rightarrow 2/3Fe_3O_4 + 1/12LaAsO_4 + 11/12LaAs. \quad (2b)$$

The reaction which is consistent with the reduction of phase fraction of LaAs is

$$Fe_2O_3 + LaAs \rightarrow 2/3Fe_3O_4 + 1/9La_2O_3 + 5/9LaAs + 2/9LaAs_2, \quad (2c)$$

which implies that the overall reaction below 400 °C is

$$LaAs + 1/3Fe_2O_3 + 1/3Fe \rightarrow 23/27LaAs + 2/9Fe_3O_4 + 1/27La_2O_3 + 2/27LaAs_2 + 1/3Fe. \quad (3)$$

Since FeO is not stable below about 570 °C, it is not necessary to consider it in the further reduction of the Fe. The complete reduction of the Fe by forming La_2O_3 would require

$$23/27LaAs + 2/9Fe_3O_4 + 1/27La_2O_3 + 2/27LaAs_2 + 1/3Fe \rightarrow 1/3LaAs + 1/3La_2O_3 + 2/3Fe + 1/3FeAs_2. \quad (4)$$

However, the observation of FeAs diffraction peaks by HEXRD and exo/endotherms in DTA at temperatures corresponding to univariant points in the Fe–As phase diagram suggests the nonequilibrium intermediate state,

$$1/3LaAs + 1/3La_2O_3 + 2/3Fe + 1/3FeAs + 1/3As. \quad (5)$$

Given the low temperature of the reaction, this state is not surprising. The presence of free arsenic is consistent with the endotherm at ~600 °C observed in the DTA curve (see Fig. 1). Not surprisingly the La_2O_3 is extremely fine grained or poorly crystallized.

The coexistence of free Fe and As, as well as FeAs makes possible the formation of all possible Fe–As compounds, FeAs, Fe_2As, $FeAs_2$, and Fe_3As_2. This explains why Fe_2As has been observed as an impurity phase. More importantly, the presence of Fe and Fe_2As can result in the formation of a liquid phase at a much lower temperature than expected from the refractory starting compositions. Although we did not identify any Fe–As compounds other than FeAs in the diffraction patterns, the DTA measurement in Fig. 1 confirms the existence of the low melting eutectic composition with an endotherm at 840 °C. Additional endotherms between 1000 and 1030 °C correspond to the melting temperatures of Fe_3As_2 and Fe_2As.[16] While Fe–As compounds other than FeAs were not observed in the diffraction patterns, this is consistent with finely dispersed fine grains, poorly crystallized grains, or relatively low phase fractions of these compounds. The latter is consistent with the size of the observed endotherm at 840 °C. The presence of liquid will accelerate the formation of LaFeAsO since a liquid phase generally increases the kinetics through increased mass transport rates. However, the formation of a liquid phase raises the potential for macroscopic phase segregation. In the extreme case of liquid formation, the Fe–As serves as a liquid phase sintering aid which causes sintering and densification of the refractory phases with limited reaction, while excess liquid is exuded from the sample in the form of metallic balls on the surface, a fairly common failure mechanism in liquid phase sintering. Once macroscopic phase segregation has occurred, there is little chance of obtaining a single-phase sample. In order to fully react the material in a reasonable amount of time, it is necessary to process in the regime of surface melting of the Fe–As without creating enough liquid that phase segregation occurs. Thus the rate at which the process temperature is ramped as well as the hold temperatures are both extremely important processing parameters. Therefore holding the samples at ~800 and ~950 °C is recommended to better homogenize the samples while minimizing the amount of phase segregation. The dwelling at 950 °C has been proven to improve the phase purity in our syntheses.

The disappearance of cubic La_2O_3 above 800 °C may be attributed to one of two possible effects: (1) cubic La_2O_3 reacts with other reactants to form LaOFeAs and (2) cubic La_2O_3 transforms to hexagonal La_2O_3 while heating. Although whether the transition is a polymorphic transition is still under debate, the cubic→hexagonal change of La_2O_3 upon heating has been observed by various groups.[19] After cooling to room temperature, the observation of hexagonal La_2O_3 suggests that cubic La_2O_3 is a metastable phase for La_2O_3.[20] The metastable, poorly crystallized cubic La_2O_3 may be more active than the hexagonal phase in the reaction with other components to form LaFeAsO.

Referring to Fig. 4, the onset of the formation of LaFeAsO is probably at ~650 °C. The strongest peaks from LaFeAsO and hexagonal La_2O_3 overlap making it difficult to determine accurately the onset temperature of LaFeAsO formation. At these relatively low temperatures, for a solid-state reaction to occur, the reactants must be in close physical proximity, ideally in contact with each other. This requires that we consider binary reactions. Given the phase compositions present above 500 °C, the only binary reactions which yields the desire phases are

$$La_2O_3 + 2FeAs \Rightarrow 2LaFeAsO + 1/2O_2 \quad (6a)$$

and

$$La_2O_3 + 2Fe_2As \rightarrow 2LaFeAsO + FeO + Fe. \quad (6b)$$

We can rule out the first reaction (6a) as it is highly unlikely that La_2O_3 will participate in a reaction with FeAs which results in the formation of free O_2 since La_2O_3 has an extremely high free energy of formation. The second (6b) is only possible for temperatures above stability limit for FeO (~570 °C) which is consistent with the lowest possible formation temperature we observed for LaFeAsO. Recalling that the La_2O_3 and Fe_2As are both products of the reaction of LaAs and Fe_3O_4, it is therefore reasonable to assume that they are well distributed and can react readily. Fe_2As may also form from the reaction of FeAs and Fe. The diffusion paths would be expected to be longer and phase formation to be slower. FeO, formed as an intermediate phase, will also react with LaAs according to

$$LaAs + FeO \rightarrow LaFeAsO. \quad (7)$$

This reaction may prevent the accumulation of significant amounts of FeO within the sample, thus preventing its detection.

According to Fig. 4, the possible phases around 650 °C are LaAs, FeAs, Fe, and La_2O_3. Thus the formation of LaFeAsO may take place via the simultaneous reaction of multiple phases. For example,

$$LaAs + La_2O_3 + 2FeAs + Fe \rightarrow 3LaFaAsO. \quad (8a)$$

While a limited amount of LaFeAsO forms between 600 and 800 °C, the rate of formation accelerates greatly above 800 °C. Recalling the Fe–Fe_2As eutectic temperature is 840 °C, a eutectic melting is expected in this temperature region and is consistent with the DTA measurements. Keeping in mind that surface melting can occur well below the bulk melting temperature,[21] the presence of liquid allows for a relatively rapid reaction of Fe_2As directly with La_2O_3, and since it is reasonable that FeO has at least limited solubility in Fe–As liquid, rapid reaction between FeO and LaAs should occur. We believe the increase in LaFeAsO formation is a direct result of liquid formation, which greatly increases the kinetics through increased mass transport rates.

On further heating, the formation of LaFeAsO plateaus above 1000 °C. The determination of the phase fractions is not possible above 1040 °C due to the fact that the FeAs has melted. After melting and resolidifying, the FeAs diffraction pattern consisted of a small number of diffraction spots. The intensity of the diffraction spots appeared to saturate the detector. Clearly the FeAs solidified as a limited number of fairly large grains and powder averaging of the pattern was not possible. In contrast, the patterns of La_2O_3 and LaFeAsO remained smooth rings characteristic of a random distribution of grains. Given a sampling volume of order of 1 mm^3, this infers a relatively fine grain size for both La_2O_3 and LaFeAsO. The inferred combination of grain sizes suggests that after melting, phase segregation has occurred. Nonetheless the final phase constitution of composition A is three-phase: LaFeAsO, La_2O_3, and FeAs.

As is suggested by the DTA (Fig. 1) and HEXRD (Fig. 4) measurements, the reaction path of the fluorine doped composition B is similar to that of the undoped composition A. The formation of the nominal $LaFeAsO_{0.9}F_{0.1}$ follows that of the undoped sample. After being heated to 1150 °C, the sample contains three phases, $LaFeAsO_{1-x}F_y$, LaOF, and FeAs. The reaction path for the incorporation of the F into the LaFeAsO matrix is not clear at this time. However, the presence of LaOF suggests that the product $LaFeAsO_{1-x}F_y$ has less fluorine than the nominal composition.

B. Stoichiometry

As discussed above, the formation of single-phase LaFeAsO and $LaFeAsO_{1-x}F_y$ presents a number of technical problems. The root cause of these problems is the fact that three to five reactants must be combined into a homogenous sample and macroscopic phase segregation must be avoided during processing. Given the fact that La_2O_3, LaF_3, LaOF, LaAs, and Fe_2O_3 all melt above 1500 °C, the diffusion of the refractory components is expected to be limited below the melting of the Fe–As phase mixtures between 840 and 1040 °C. However, the results of the x-ray experiments indicate that there is a more fundamental problem in obtaining single-phase materials.

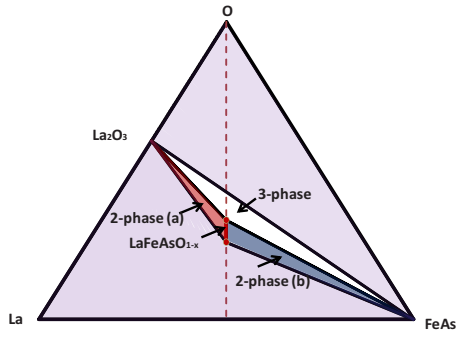

FIG. 8. (Color online) Ternary cut through the La–Fe–As–O quaternary phase diagram showing the solid solution $LaFeAsO_{1-x}$, the two phase region La_2O_3–$LaFeAsO_{1-x}$ (a), the two phase region FeAs–$LaFeAsO_{1-x}$ (b), and the three phase region La_2O_3–$LaFeAsO_{1-x}$–FeAs. The remainder of the cut consists of four-phase regions containing at least one phase not in the plane of the cut.

An examination of the observed phase composition of the reacted samples shows that this phase distribution cannot be a result of a complete reaction if the LaFeAsO phase is assumed to be stoichiometric or the atomic ratio in the starting materials are exactly 1:1:1:1 for La:Fe:As:O. While this conclusion is based on assuming that all phases present in the sample are observed, we will discuss the extent to which other phases must be present to invalidate the conclusion in the following analysis. For the undoped case, the impurity phases are La_2O_3 and FeAs. If these two phases were to react to form LaFeAsO, the reaction would be

$$\tfrac{1}{2}La_2O_3 + FeAs \Rightarrow LaFeAsO + 1/4O_2. \quad (8b)$$

Similarly for the doped case the reaction would be

$$LaOF + FeAs \Rightarrow LaFeAsO_{1-x}F_y + \{\text{excess O and F}\}, \quad (8c)$$

where $x=y$. As discussed above, the high stability of rare earth oxides, fluorides, and oxyfluorides makes these reactions highly unlikely, and even if they did occur, it is clear that there is an excess of O in the case of the undoped material or an excess of O and F for the F-doped material.

The implications of this are most easily explained for the undoped case. In Fig. 8, a cut through the four-phase equilibrium phase diagram of La–Fe–As–O is presented. The cut is the plane determined by La, O, and FeAs. Fortunately LaFeAsO also lies in this plane as does the three-phase triangle La_2O_3, FeAs, LaFeAsO. Outside of this triangle are multiple four-phase regions containing phases which do not lie in the plane. In our high temperature x-ray scans versus temperature, the only phases which appear are those of the three-phase triangle. If the LaFeAsO is stoichiometric and the samples were not fully reacted, the presence of one or more phases containing La and As but very little O is required to react with the observed La_2O_3 and FeAs. From the diffraction patterns, the amount of these phases must be less than 1 wt %, which is insufficient to balance the observed impurity phases. As a result, the only viable alternative is

TABLE I. Phase fractions for starting composition A with no F, LaFeAsO. The values of the observed weight percentage of the detected phases based on Rietveld refinement of the 1040 °C diffraction pattern compared to the calculated phase fractions obtained by least squared fitting the phase fractions by varying x for $LaFeAsO_{1-x}F_y$. The best fit to the relative phase fractions is for $x=0.32$.

	Rietveld results (wt %)	Calculated phase fractions for $x=0.32$ (wt %)
$LaFeAsO_{1-x}$	60(1)	60
FeAs	18(5)	18
La_2O_3	22(5)	22

that the LaFeAsO phase forms at an oxygen deficient composition, $LaFeAsO_{1-x}$. If we assume that $LaFeAsO_{1-x}$ exists over a range of values of x, while maintaining the 1:1:1 La:Fe:As ratio, the solid solution lies in the plane of the cut along the line from O to the 50-50 composition on the La–FeAs tie line as indicated in Fig. 8 where the extent of the solid solution is defined to be in the range $a \leqslant x \leqslant b$ where the values of the positive variables a and b are not specifically specified. The equilibrium three-phase triangle is now La_2O_3, FeAs, $LaFeAsO_{1-a}$. For a starting composition of 1:1:1:1, the equilibrium phase distribution is

$$1/(1+3a)LaFeAsO_{1-a} + x/(1+3a)La_2O_3 + 2a/(1+3a)FeAs. \quad (9a)$$

However, a nonequilibrium distribution of the three phases may be observed for $a \leqslant x \leqslant b$ with phase fractions,

$$1/(1+3x)LaFeAsO_{1-x} + x/(1+3x)La_2O_3 + 2x/(1+3x)FeAs. \quad (9b)$$

In this case, further reaction between the $LaFeAsO_{1-x}$, La_2O_3, and FeAs is possible until $x=a$ at which point the reaction is complete leaving $a/(1+3a)$ mole fraction of La_2O_3 and $2a/(1+3a)$ mole fraction of FeAs as impurity phases as given by Eq. (9a).

Based on the phase fractions determined from Rietveld refinement of the x-ray scan, we can calculate the value of x. As can be seen in Table I, the calculated phase fractions for $1-x=0.68$ are in excellent agreement with the experimental fractions of $LaFeAsO_{1-x}$ (60 wt %), FeAs (18 wt %), and La_2O_3 (22 wt %). If the starting composition lies within the $LaFeAsO_{1-x}$–FeAs–La_2O_3 three-phase triangle and the reaction is complete, then $x=a$. If the starting composition lies within the three-phase triangle and the reaction is not complete, then the O content of the 1111 somewhere between $1-b$ and $1-a$.

For the undoped material, the multiphase region containing the starting composition was a three-phase triangle in a ternary cut shown in Fig. 8 through the quaternary diagram and the graphical representation of the phase field was clear. For the case of fluorine doping the analysis becomes somewhat more complicated as both the O and F concentrations may vary. With the addition of F a multiphase composition no longer lies in the three-phase triangle but rather in a five-phase region where the limits of the solid solution

TABLE II. Phase fractions for starting composition B with F, $LaFeAsO_{0.9}F_{0.1}$. The values of the observed weight percentage of the detected phases based on Rietveld refinement of the 1040 °C diffraction pattern compared to the calculated phase fraction obtained by fitting the phase fractions by varying x and y for $LaFeAsO_{1-x}F_{1-y}$. The best fit value is $x=0.113$ and $y=0.014$. Given the small value of y, the data were also fit forcing $y=0$ which yielded $x=0.11$.

	Rietveld results (wt %)	Calculated phase fractions for $x=0.11$, $y=0$ (wt %)	Calculated phase fractions for $x=0.113$, $y=0.014$ (wt %)
$LaFeAsO_{1-x}F_y$	90(1)	89	90
LaOF	6.5(5)	6.1	5.3
FeAs	2.0(5)	4.6	4.3
La_2O_3	1.5(5)	0	0.2

$LaFeAsO_{1-x}F_y$ are not known. However, the phase fractions of the five constituents may be determined for any allowable pair of x and y by solving five linear equations for five unknowns. The values of x and y are then determined by a least squares fit to the phase fractions determined from Rietveld refinement of the x-ray scan at 1040 °C for composition B. In Table II, the observed and calculated values are given. The first observation is that the value of 6.5 wt % for LaOF is greater than the 6.1 wt % which can be formed if all of the F is consumed in the LaOF. While this is well within the uncertainty of the phase fraction determination of the refinement, it implies that y is very small or zero. If we apply the constraint that $y=0$, then $x=0.11$. Allowing both x and y to vary returns a slightly better fit with $x=0.113$ and $y=0.014$. Given the difficulty of determining the phase fractions at such low levels, the difference between the fits is negligible. As with the undoped case, we only know that these are allowable values within the range of solid solution and may depend on the completeness of the reaction.

Our evaluation of the x for compositions A and B have yielded two very different answers with a relatively large value ~0.3 for the F-free composition A and a much smaller value of ~0.1 for the F-containing composition B. Since under our processing conditions, very little or no F entered into the $LaFeAsO_{1-x}F_y$ compound we can infer that in $LaFeAsO_{1-x}$, x can be as small as that observed in composition B. Thus we draw the conclusion that, at a minimum, the solid solution $LaFeAsO_{1-x}$ exists over the range $0.1 \leqslant x \leqslant 0.3$ (Table II). However, we cannot draw conclusions as to the extent, if any, of the possible F substitution. In addition it is important to note that for a starting composition of $LaFeAsO_{0.9}F_{0.1}$, standard laboratory x-ray diffraction measurements, with a detection limit of around 5 wt %, are hard pressed to differentiate between a sample with a fully occupied O site and one with an occupation of 0.9.

V. CONCLUSIONS

We have identified the reaction path for the formation of the FeAs based superconductors $LaFeAsO_{1-x}$ and $LaFeAsO_{1-x}F_y$ and shown that the control of the reaction in the proximity of the Fe–Fe_2As eutectic temperature is im-

portant for controlling the reaction rates and sample homogeneity. More importantly we have shown that the materials can form over range of oxygen stoichiometry at high temperature. The oxygen content is highly dependent on the completeness of the reaction. Our ability to determine the secondary phase content and hence the oxygen content of the sample using standard laboratory x-ray diffraction patterns is limited. This oxygen variability plays a significant role in the phase formation and may control the amount of F which is actually doped into the sample. While this fact controls the ability to make single-phase samples, it also significantly alters the understanding of the doping of the FeAs planes in nominal $R\mathrm{FeAsO}_{1-x}\mathrm{F}_x$.

ACKNOWLEDGMENTS

The assistance of D. S. Robinson in performing the HEXRD studies at the APS was essential to the completion of this work and is gratefully acknowledged. The work at Ames Laboratory and at the MU-CAT sector was supported by the U.S. DOE under Contract No. DE-AC02-07CH11358. Use of the Advanced Photon Source was supported by U.S. DOE under Contract No. DE-AC02-06CH11357.

[1]Y. Kamihara, T. Watanabe, M. Hirano, and H. Hosono, J. Am. Chem. Soc. **130**, 3296 (2008).
[2]N. Ni, S. L. Bud'ko, A. Kreyssig, S. Nandi, G. E. Rustan, A. I. Goldman, S. Gupta, J. D. Corbett, A. Kracher, and P. C. Canfield, Phys. Rev. B **78**, 014507 (2008).
[3]N. Ni, S. Nandi, A. Kreyssig, A. I. Goldman, E. D. Mun, S. L. Bud'ko, and P. C. Canfield, Phys. Rev. B **78**, 014523 (2008).
[4]J.-Q. Yan, A. Kreyssig, S. Nandi, N. Ni, S. L. Bud'ko, A. Kracher, R. J. McQueeney, R. W. McCallum, T. A. Lograsso, A. I. Goldman, and P. C. Canfield, Phys. Rev. B **78**, 024516 (2008).
[5]X. F. Wang, T. Wu, G. Wu, H. Chen, Y. L. Xie, J. J. Ying, Y. J. Yan, R. H. Liu, and X. H. Chen, Phys. Rev. Lett. **102**, 117005 (2009).
[6]R. Morinaga, K. Matan, H. S. Suzuki, and T. J. Sato, J. Phys. Soc. Jpn. **48**, 013004 (2009).
[7]For example, G. F. Chen, Z. Li, G. Li, J. Zhou, D. Wu, J. Dong, W. Z. Hu, P. Zheng, Z. J. Chen, H. Q. Yuan, J. Singleton, J. L. Luo, and N. L. Wang, Phys. Rev. Lett. **101**, 057007 (2008).
[8]I. Nowik and I. Felner, J. Supercond. Novel Mater. **21**, 297 (2008).
[9]M. A. McGuire *et al.*, Phys. Rev. B **78**, 094517 (2008).
[10]R. M. German, *Liquid Phase Sintering* (Plenum, New York, 1985).
[11]Materials Preparation Center, Ames Laboratory US-DOE, Ames, IA.
[12]Y. Janssen, M. Angst, K. W. Dennis, P. C. Canfield, and R. W. McCallum, Rev. Sci. Instrum. **77**, 5 (2006).
[13]L. Margulies, M. J. Kramer, R. W. McCallum, S. Kycia, D. R. Haeffner, J. C. Lang, and A. I. Goldman, Rev. Sci. Instrum. **70**, 9 (1999).
[14]A. P. Hammersley, ESRF Internal Report No. ESRF97HA02T, 1997.
[15]A. Larson and R. B. von Dreele, The Regents of the University of California, Los Alamos 1985.
[16]As–Fe Phase Diagram, Alloy Phase Diagrams/,/Volume 3, ASM Handbook Handbook (online). http://products.asminternational.org/hbk/index.isp.
[17]V. W. Klemm and H. A. Klein, Z. Anorg. Allg. Chem. **248**, 167 (1941).
[18]L. S. Darkin and R. W. Gurry, J. Am. Chem. Soc. **68**, 798 (1946).
[19]M. Zinkevich, Prog. Mater. Sci. **52**, 597 (2007) and references therein.
[20]G.-y. Adachi and N. Imanaka, Chem. Rev. (Washington, D.C.) **98**, 1479 (1998).
[21]J. G. Dash, Contemp. Phys. **30**, 89 (1989).